Thermohydraulic Dynamics and Fuzzy Coordination Control of a Microchannel Cooling Network for Space Electronics

Yun-Ze Li, *Member, IEEE*, and Kok-Meng Lee, *Fellow, IEEE*

***Abstract*—This paper presents the dynamic model, analysis, and fuzzy control of a microchannel-heat-exchanger (MHE) space cooling network for dissipating exhaust heat of onboard electronic components inside spacecraft to the outer space environment. Along with a method for modeling a nonlinear fluid resistance network, a detailed analysis of flow rate changes and temperature transients of the MHE cooling network is given, providing a basis for developing a fuzzy coordination control strategy. The fuzzy controller employs two synergic PID controllers to simultaneously control both fluid- and radiation-based cooling mechanisms. The fuzzy coordination controller has been numerically evaluated, demonstrating a better performance than single-input PID controllers in terms of its ability to leverage between two actuators in rejecting disturbances and preventing overmanipulation. This unique feature will benefit the operating reliability of the MHE cooling network under stiff space working conditions.**

***Index Terms*—Dynamic model, fuzzy control, microchannel heat exchanger (MHE), space cooling network, thermohydraulics.**

I. Introduction

MICROCHANNEL heat exchangers (MHEs) have been widely employed in the cooling and thermal management of ground-based electronic systems with high power density (like high-heat-flux insulated-gate bipolar transistors [1], high-power diode laser bars [2], and printed circuit boards [3]). Because of their compact structure and light weight, they are also very promising in an advanced thermal control architecture for future spacecraft and space applications (micro- and nanosatellites in near-Earth orbits [4] and Mars landers [5]) and other interplanet missions, where networked MHEs are required to dissipate exhaust heat from multiple high-power-density electronic units. In general, many high-power-density electronic units, including avionics (onboard processors and power and inertial management units), telecom (solid-state power amplifier, deep space transponder, and UHF transmitter), and science payload, are needed on a modern practical spacecraft [4], [5]. A multiexchanger network is often required to gather exhaust heat from different electronic units and dissipate the heat into the space environment [6], [7] by radiation. Successful development of an MHE cooling network for space applications requires a good understanding of its thermohydraulic dynamics.

Significant research effort has been focused on MHEs with liquid-state cooling fluid [4], [5] for their easy design and safety operating characteristics [8] that make them more suitable for aerospace applications. Among these, some MHEs integrated in a single-phase pumped cooling loop with water as the working fluid [4], [5], [8] for the thermal and hydraulic performance have been demonstrated to have heat-removing ability of up to 25 W/cm^2 and can meet hydraulic performance criteria, requiring less than 1-lb/in^2 pressure drop. However, most of the recently reported investigations focused on the flowing mechanics [9], [10] and heat transferring phenomenon [11], [12] inside the MHEs. Based on these, optimal design models and related algorithms have been developed to improve thermohydraulic performances at a system level, including energy efficiency, weight, volume, and manufacturability [13], as well as to optimize exchanger level parameters like pressure drop and thermal resistance [14]. Relative researches that focused on similar traditional size heat exchanger networks include analog dynamic simulation techniques for mass flow rate distribution analysis in [15], model reduction control strategies [16], and predictive control algorithms in [17]. Fuzzy-logic-based intelligent controls (which have been successfully demonstrated for controlling moving objects [18] and electric machines [19]–[21]) also show promises to improve control performances of thermal-fluid systems; for example, gas-turbine plants [22], MHEs [23], water-bath cooling systems [24], and, more recently in [25], fuzzy logic units are used for the high-precision control of a thermoelectric cooler and its cooling fan.

A space MHE cooling network is a complex nonlinear thermohydraulic system consisting of a fluid network and a space radiator (with variable emissivity coatings [8] and, more recently, micromachined louver assay [7]); its dynamic modeling and control system design are challenging. Conventional PID controllers employing a single input have a number of practical drawbacks, which include frequent adjustment of the louver array (on the outer surface of the space radiator) and significantly reduce the reliability of the thermal control system. On the other hand, the fast hydraulic-based PID control often

Manuscript received August 12, 2009; revised January 15, 2010; accepted March 3, 2010. Date of publication March 22, 2010; date of current version January 12, 2011. This work was supported in part by the National Natural Science Foundation of China under Grant 50506003 and in part by the Aeronautic Science Foundation of China under Grant 2008ZC51028.

Y.-Z. Li is with the School of Aeronautical Science and Engineering, Beihang University, Beijing 100191, China (e-mail: liyunze@buaa.edu.cn).

K.-M. Lee is with The George W. Woodruff School of Mechanical Engineering, Georgia Institute of Technology, Atlanta, GA 30332-0405 USA (e-mail: kokmeng.lee@me.gatech.edu).

Color versions of one or more of the figures in this paper are available online at http://ieeexplore.ieee.org.

Digital Object Identifier 10.1109/TIE.2010.2045999

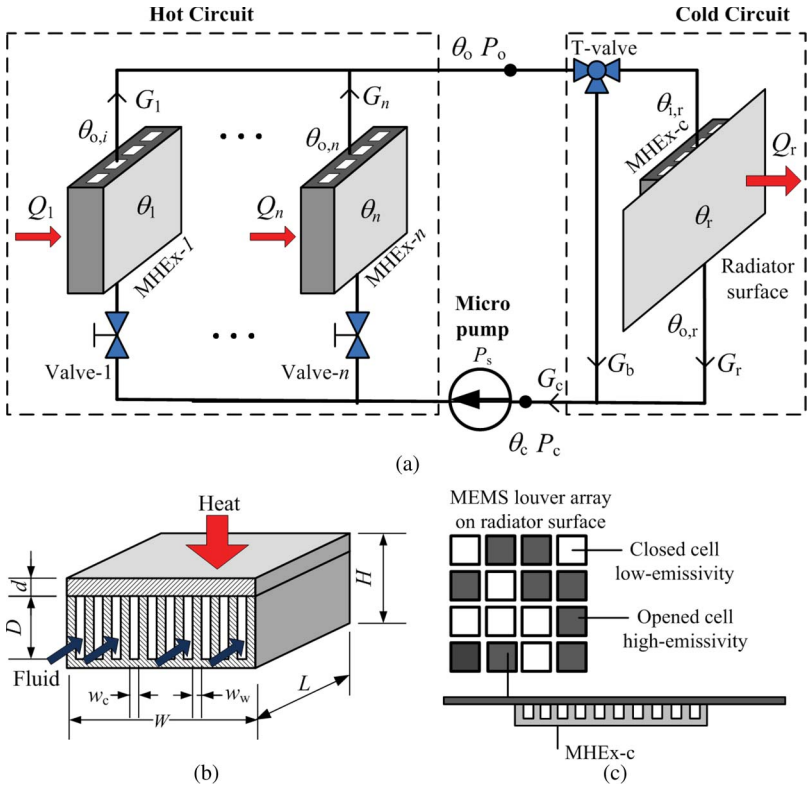

Fig. 1. Space cooling network configuration. (a) Space cooling network. (b) MHEx. (c) MEMS louver array.

introduces undesired hydraulic disturbances in the MHEs and is only suitable for applications where disturbance is small. For these reasons, we present here an improved controller that takes into account the dynamic characteristics of the hydraulic and thermal actuators to overcome problems associated with single-input PID controls.

The remainder of this paper offers the following.

1) Along with a method for modeling a nonlinear fluid resistance network, the thermohydraulic dynamic model of a cooling network which consists of MHEs, a fluid bypass, and a micro-electromechanical system (MEMS) based louver array is provided.
2) A detailed analysis is performed to investigate the effects of key manipulating inputs, and disturbances (due to flow rate variation and heat load changes) on temperature transients of the MHE cooling network are discussed.
3) A fuzzy coordination strategy, which employs two synergic PID controllers to leveraging between two inputs, a fluid-based cooling system and a radiation-based one, is derived and numerically evaluated against two single-input PID controllers.

II. System Description and Dynamical Modeling

Fig. 1 shows a space cooling network of MHEs [Fig. 1(b)] with a MEMS louver array [Fig. 1(c)]. The cooling network typically includes a hot circuit, a cold circuit, and a micropump.

1) The *hot circuit* is composed of one or more MHEs (denoted as MHEx-1, . . . , MHEx-i, . . . , MHEx-n in Fig. 1) mounted on high-power-density electronic components,

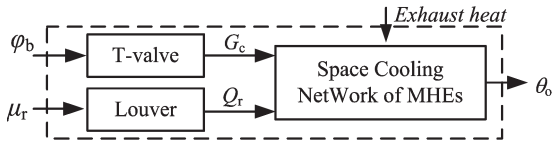

Fig. 2. Block diagram representing the space cooling network.

where exhaust heat is transferred into the cold fluid as it flows through the MHEs to the cold circuit.
2) In the *cold circuit*, the fluid temperature decreases as it flows through MHEx-c, where heat is removed from the heated fluid to the outer space through a MEMS louver array on the space radiator located outside of the spacecraft.
3) The micropump recycles the single-phase working fluid between the hot and cold circuits.

Without loss of generality, in the following discussion, pure water (with specific heat c_w) is assumed, and temperature is in degrees Celsius (°C).

The objective is to control the temperature θ_o at the hot circuit outlet regardless of the changes in electronic heat load or in hydraulic facts such as inlet flows through the MHEs in the hot circuit. As illustrated by the block diagram in Fig. 2, the cold circuit offers two mechanisms to control the hot circuit temperature θ_o, namely, the MEMS louver array at MHEx-c and the bypass channel of the three-way T-valve at the entrance of the cold circuit.

MEMS Louver Array: As shown in Fig. 1(c), the two surfaces of each louver cell are coated such that the surface emissivity is low when fully closed and high when fully opened. The heat transfer mode at the outer radiator surface

is dominated by radiation since there is no air surrounding the spacecraft in the orbit environment. Thus, the cooling capacity of the network can be effectively set by opening an appropriate number of louver cells. We define the exposing degree μ_r of the radiator surface as the ratio between the exposed area under the opened louver cells and the total area of the radiator surface. Mathematically, the heat flux leaving the radiator is given by

$$Q_r = \varepsilon_e \sigma A_r (\theta_r + \delta)^4, \qquad \text{where } \varepsilon_e = (\varepsilon_h - \varepsilon_l)\mu_r + \varepsilon_l \quad (1)$$

σ is the Stefan–Boltzmann constant, and A_r and θ_r are the total area and the average temperature ($\delta = 273.15$) of the space radiator surface, respectively. In (1), the equivalent radiator emittance ε_e is approximated as a linear function of the low and high surface emittances (denoted respectively as ε_l and ε_h) of the louver cell with μ_r as a controlling variable.

Bypass Channel of the Three-Way T-Valve: As shown in Fig. 1(a), the flow distribution at the cold circuit inlet is controlled by a three-way T-valve. The T-valve can be modeled hydraulically as two independent two-way valves in parallel such that the mass flows through the bypass channel and MHEx-c are proportional to φ_b and $(1 - \varphi_b)$, respectively, where φ_b is the manipulating variable of the T-valve.

A. Fluid Flow Model

For a typical MHE space cooling system, the fluid flow system has a much smaller time constant than its thermal system dynamically and is neglected in system modeling. For clarity in illustration and providing a basis for performance analysis, we model the valve, MHEs, and associated inlet/outlet pipes, which are connected in series in a branch, as a nonlinear flowing element satisfying the relationship

$$G = \varphi\sqrt{\Delta P/R} = \sqrt{\Delta P/R_{\text{eq}}}, \qquad \text{where } R_{\text{eq}} = R/\varphi^2 \quad (2)$$

and where ΔP and G are the pressure difference across and the mass flow rate through the element, respectively, the parameter φ characterizes the valve opening, and R is the flow resistance of the MHE and associated inlet/outlet pipes. For a fluid circuit consisting of n such branches in parallel or in series, the overall resistance R_{net}, the total pressure drop ΔP_{net}, and the mass flow rate G_{net} across the fluid network, as well as the flow rate distribution law for each branch, can thus be derived using nonlinear circuit theory; the results are summarized in Table I, where $1 \le i \le n$.

From Fig. 1(a), the mass flow rate through the micropump for a given pressure supply P_s can be written as

$$G_c = \sqrt{P_s/(R_h + R_c)} \quad (3)$$

where R_h and R_c are the effective flow resistances that characterized the hot and cold circuits, respectively. Using Table I, the flow resistance across the hot circuit is given by

$$\frac{1}{\sqrt{R_h}} = \frac{\varphi_1}{\sqrt{R_1}} + \cdots + \frac{\varphi_i}{\sqrt{R_i}} + \cdots + \frac{\varphi_n}{\sqrt{R_n}}. \quad (4)$$

Since the three-way T-valve at the inlet of the cold circuit can be treated hydraulically as two independent two-way valves (with valve opening variables φ_b and $1 - \varphi_b$ and branch resistances R_b and R_r, respectively) in parallel, the flow resistance across the cold circuit can be written as

$$\frac{1}{\sqrt{R_c}} = \frac{1 - \varphi_b}{\sqrt{R_r}} + \frac{\varphi_b}{\sqrt{R_b}}. \quad (5)$$

The corresponding mass flow rates through MHEx-i, MHEx-c, and the bypass channel (G_i, G_r, and G_b, respectively) are given by

$$\frac{G_i}{G_c} = \varphi_i\sqrt{\frac{R_h}{R_i}} \quad (6a)$$

$$\frac{G_r}{G_c} = (1 - \varphi_b)\sqrt{\frac{R_c}{R_r}} \quad (6b)$$

$$\frac{G_b}{G_c} = \varphi_b\sqrt{\frac{R_c}{R_b}}. \quad (6c)$$

TABLE I
NONLINEAR PARALLEL AND SERIES FLOW NETWORK

	Parallel	Series
R_{net}	$\left(\sum_{i=1}^{n} \varphi_i / R_i^{-1/2}\right)^{-2}$	$\sum_{i=1}^{n} R_{\text{eq},i} = \sum_{i=1}^{n} \left(R_i/\varphi_i^2\right)$
ΔP_{net}	ΔP_i	$\sum_{i=1}^{n} \Delta P_i = R_{\text{net}} G_i^2$
G_{net}	$\sum_{i=1}^{n} G_i = \sqrt{\Delta P_{\text{net}}/R_{\text{net}}}$	G_i
G_i / G_{net}	$\varphi_i\sqrt{R_{\text{net}}/R_i}$	1

B. Heat Transfer and Temperature Dynamic Model

The temperature dynamics of the space cooling system are contributed by three sources: the radiator in the cold circuit, the n MHEs in the hot circuit, and the working fluid recycling in the network.

For compactness in presentation, a general effectiveness of an MHE is defined in

$$\xi_x = (\theta_{i,x} - \theta_{o,x})/(\theta_{i,x} - \theta_x) \quad (7)$$

where θ_x, $\theta_{i,x}$, and $\theta_{o,x}$ are the temperatures for the structure and the inlet and outlet water of the MHE being considered, respectively, and the subscript $x \in \{r, i\}$ represents MHEx-c with the radiator and MHEx-i in the hot circuit, respectively. The value of the effectiveness can be calculated from

$$\xi_x = 1 - \exp\left[-(\eta_x h_x A_{h,x})/(G_x c_w)\right] \quad (8)$$

where G_x and c_w are the mass flow rate and the specific heat of the water flowing through the MHE, respectively, and η_x, h_x, and $A_{h,x}$ are the fin efficiency, convective heat transfer coefficient, and area of it, respectively. Note that the walls between the micro flowing channels are modeled as fins. This is a widely accepted approximation when rectangle flowing channels are involved in a small-size heat exchanger (see [1]).

Cold Circuit Dynamics: The radiator temperature θ_r is governed by the conservation of energy in

$$M_r c_r \dot{\theta}_r = G_r c_w \xi_r (\theta_{i,r} - \theta_r) + A_r \sum_{j=1}^{3} \alpha_j q_j - Q_r \qquad (9)$$

where M_r and c_r are the mass and specific heat of MHEx-c and its connected surface radiator, respectively, $\theta_{i,r}$ is the inlet temperature of the water flowing through MHEx-c with effectiveness ξ_r in (7) and (8), the heat flux Q_r leaving the radiator is given in (1), and α_j and q_j are the absorptance and input radiant heat flux density at the radiator's outer surface, respectively, where the subscripts "$j = 1, 2, 3$" denote the contributions from the solar radiation, Earth radiation, and albedo (or the Earth surface reflectivity of sun radiation), respectively. The values of q_j are determined by the in-orbit position and attitude of the spacecraft [26].

The water temperature θ_c at the cold circuit exit can be calculated by

$$(M_c \bar{c}_c)\dot{\theta}_c = G_r c_w (\theta_{o,r} - \theta_c) + G_b c_w (\theta_o - \theta_c) \qquad (10)$$

where M_c and $\bar{c}_c$ are the total mass and the average specific heat of the cold circuit pipe and working fluid system, respectively, and $\theta_{o,r}$ is the water outlet temperature of MHEx-c given by

$$\theta_{o,r} = \theta_{i,r} - \xi_r (\theta_{i,r} - \theta_r). \qquad (11)$$

Hot Circuit Dynamics: Similarly, the dynamics of the ith exchanger (MHEx-i) temperature θ_i is given by

$$M_i c_i \dot{\theta}_i = Q_i - \xi_i G_i c_w (\theta_i - \theta_{i,i}) \qquad (12)$$

where M_i and c_i are the mass and specific heat of MHEx-i, respectively, Q_i is the exhaust heat input, and $\theta_{i,i}$ is the inlet temperature of the water flowing through MHEx-i with effectiveness ξ_i in (7) and (8).

The exit water temperature θ_o of the hot circuit can be computed from (8)

$$(M_h \bar{c}_h)\dot{\theta}_o = c_w \sum_{i=1}^{n} G_i (\theta_{o,i} - \theta_o) \qquad (13)$$

where M_h and $\bar{c}_h$ are the total mass and average specific heat of the hot circuit pipes and working fluid, respectively, and

$$\theta_{o,i} = \theta_{i,i} + \xi_i (\theta_i - \theta_{i,i}). \qquad (14)$$

Thermohydraulic Dynamics: Neglecting the heat loss of the pipes in both the hot and cold circuits

$$\theta_{i,i} \approx \theta_c \qquad \theta_{i,r} \approx \theta_o. \qquad (15)$$

The thermohydraulic dynamics of the space cooling network can be expressed in state-space form consisting of $n + 3$ state equations with two inputs

$$\dot{\mathbf{X}} = \mathrm{F}(\mathbf{X}, \mathbf{Q}, \mathrm{g}(\varphi_b, P_s), \Gamma(\mu_r)) \qquad (16)$$

where $\mathbf{X} = [\theta_1, \ldots, \theta_i, \ldots, \theta_n, \theta_r, \theta_o, \theta_c]^{\mathrm{T}}$ is the state variable vector, $\mathbf{Q} = [Q_1, \ldots, Q_i, \ldots, Q_n]^{\mathrm{T}}$ is the heat load vector, the vector function $\mathrm{F}()$ represents the temperature dynamic models in (9)–(15), the vector function $\mathrm{g}()$ consists of the nonlinear hydraulic equations from (3)–(6), and $\Gamma()$ is the radiator's cooling ability function defined in the nonlinear equation (1).

TABLE II
VALUES OF MHE SPACE COOLING NETWORK PARAMETERS

Parameter (Unit)	Symbol	Value
MHE		
Channel depth and width (μm)	$D \times w_c$	350×100
Channel space (μm)	w_w	120
Channel length (cm)	L	2
Working Fluid		
Average density (kg/m^3)	ρ_f	983.2
Specific heat (kJ/(kg.℃))	c_f	4.179
Mass flow-rate MHEx-*1,2* (kg/s)	G_1, G_2	0.983×10^{-2}
Mass flow rate in MHEx-*c* (kg/s)	G_r	1.181×10^{-2}
Space Cooling network		
Number of MHEs in hot circuit		2
Number of MHE in cold circuit		1
Heat load of MHEx-*1,2* (W)	Q_1, Q_2	205.4
T-valve bypass value	φ_b	0.15
Radiator's exposing degree	μ_r	0.9

C. Simulation of Cooling Network Dynamics

As an illustration, we numerically simulate an MHE space cooling network with geometric parameters and initial operating parameters given in Table II. The interest is to investigate the effects of key parameters on the temperature. Four cases are considered.

Fluid Flow Variation:

Case I (hot circuit flow variation): a 20% step reduction in the inlet valve value φ_1 to MHEx-1.

Case II (cold circuit flow variation): a 10% step reduction in the bypass value φ_b at the inlet of the T-valve.

Heat Flow Variation:

Case III (cold circuit radiation): a 10% step reduction in the exposing degree μ_r of the space radiator.

Case IV (hot circuit load): a 10% step increase in the heat load Q_1 to MHEx-1.

The simulated step responses illustrating the hydraulic effects on the temperature dynamics are graphed in Fig. 3, where the left and right columns correspond to Cases I and II, respectively. The effects of the four cases on fluid and MHEx temperatures are compared in Figs. 4 and 5, respectively. For ease of comparison, Table III summarizes the settling time of the state variables. As the disturbances caused by the reduction in the inflow to MHEx-1 (Case I) are much smaller than those in the other three cases (II, III, and IV), 1% criterion is used for the settling time for Case I and 2% criterion for the other cases in Table III.

The results offering some insights are summarized as follows.

Case I (Left Column of Fig. 3): A 20% step reduction in MHEx-1 inlet opening results in an 8.7% decrease in G_r, a slight 2.7% increase in G_2, and a direct 20.1% drop in G_1. As a result, the following are observed.

1) The average MHEx-1 temperature rises sharply, while that of MHEx-2, it immediately decreases and then

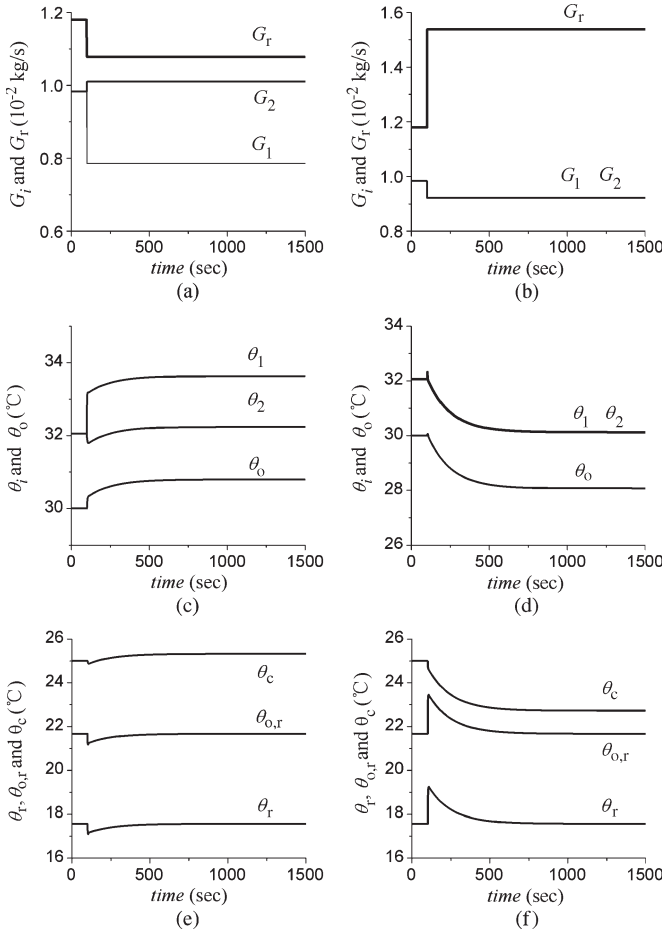

Fig. 3. Hydraulic effects on temperature responses. Left column: (a), (c), and (e) for Case I. Right column: (b), (d), and (f) for Case II.

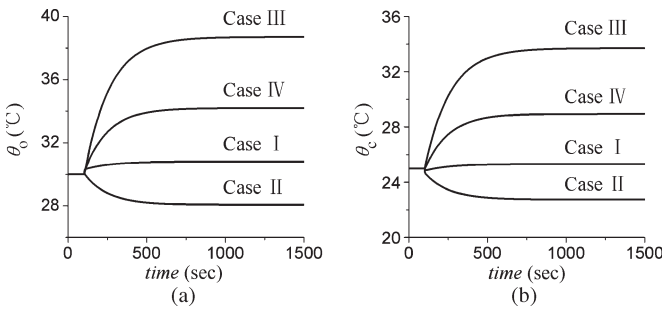

Fig. 4. Temperature responses of working fluid. (a) Hot outlet. (b) Cold outlet.

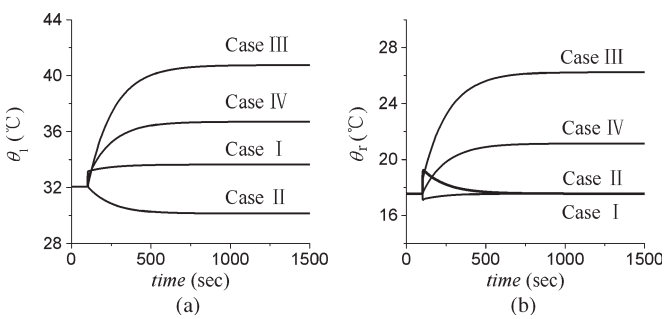

Fig. 5. Temperature responses of heat exchangers. (a) MHEx-1. (b) Radiator.

TABLE III
SETTLING TIME OF THE STATE VARIABLES

Cases	Settling time in sec. (1% criterion for I; 2% criterion for II, III, IV)				
	θ_1	θ_2	θ_r	θ_c	θ_o
I	61	99	131	127	78
II	163	163	250	225	174
III	377	377	427	405	416
IV	258	267	323	284	266

exponentially increases to a new steady state; the final changes are 4.9% and 0.6% when the respective settling times are 61 and 99 s.

2) A short but sharp temperature drop can also be observed at the MHEx-c outlet. However, the radiator temperature slowly returns to its initial value (with a settling time of 131 s) since the total heat load of the cooling network remains unchanged.
3) The working fluid temperature at the cold circuit outlet drops slightly and then climbs to a new steady-state value 1.2% higher than its initial value, while the hot circuit outlet temperature increases to a higher steady-state value after its immediate 2.6% climb up. The settling times are 127 and 78 s, respectively. This slows the increase of θ_c, resulting in the later stage increase of the temperature of hot circuit MHEs, θ_1 and θ_2 in Fig. 3.

Case II (Right Column of Fig. 3): The 10% step reduction in the T-valve bypass increases G_r by 30.3% and is accompanied with a 6.3% decrease in G_1 and G_2.

1) Because of a sudden increase in the mass flow rate through MHEx-c, the radiator temperature θ_r and its fluid outlet temperature $\theta_{\rm ro}$ rise, but the short transients die immediately and then drop to their initial values exponentially.
2) The exponential decrease in the fluid temperature θ_c at the cold circuit outlet results in lowering θ_o, θ_1, and θ_2 in the hot circuit to new steady values. The respective drops are 6.4% for θ_o and 6.1% for θ_1 and θ_2.
3) The thermal and hydraulic parameter changes in Case II are more obvious than that in Case I according to Fig. 3 and the respective settling time values in Table III.

Effect on Fluid Temperature (Fig. 4):

1) The fluid temperatures at both hot and cold circuit outlets respond more quickly to flow changes (Cases I and II) than thermal changes (Cases III and IV). The change in MEMS louvers (Case III), however, has a dominant effect on the steady-state value of the fluid temperature.
2) The absolute final fluid temperature change of θ_o in Case II is only 22.8% of that in Case III, and the respective settling time ratio between same cases is 41.8%, according to the results in Table III and Fig. 4.
3) The aforementioned one suggests that the T-valve is more useful for rapid rejection of small disturbances, but the radiator is more suitable for settling of large disturbances, as changing the valve opening to hot circuit MHEs is relatively ineffective to the global operating parameters such as θ_o and θ_c.

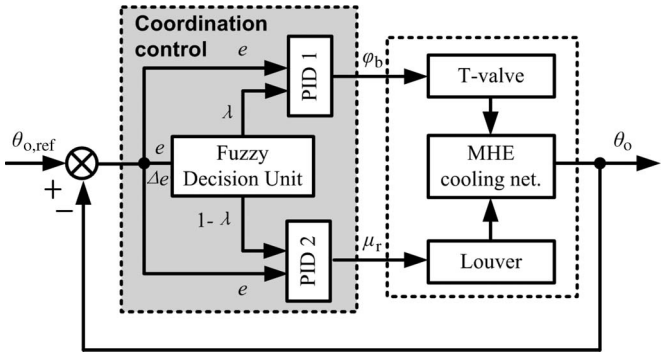

Fig. 6. Fuzzy coordination control.

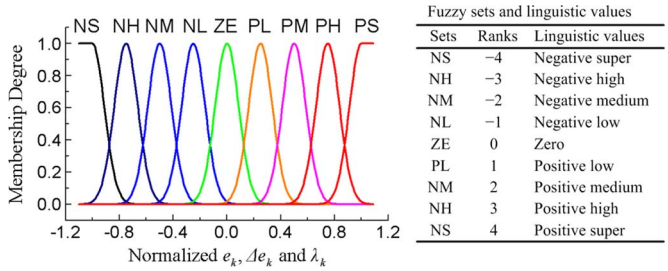

Fuzzy sets and linguistic values

Sets	Ranks	Linguistic values
NS	−4	Negative super
NH	−3	Negative high
NM	−2	Negative medium
NL	−1	Negative low
ZE	0	Zero
PL	1	Positive low
NM	2	Positive medium
NH	3	Positive high
NS	4	Positive super

Fig. 7. Fuzzy sets and membership degree functions.

Effect on MHE Temperature (Fig. 5):

1) The MHEx-1 temperature increases to step changes defined in Cases I, III, and IV but decreases to step change in the bypass (Case II).
2) The steady radiator temperature is insensitive to Cases I and II, since there is no change in the total heat load or radiation cooling, but settles to a new steady state higher than its initial value in response to Case III or IV (due to the decrease in radiation cooling or increase in heat load); the final steady value changes are 49.4% and 20.1%, respectively.
3) The adjustment of the exposing degree must be employed when strict working temperature range is required for the safe operation of the MEMS radiator according to the aforementioned observations.

III. Fuzzy Coordination Control

A safe temperature range is often required for reliable working of onboard electronic components cooled by the space cooling network; the fluid temperature at the hot circuit outlet is chosen as the controlled variable since it reflects the impacts of different MHEs more reasonably than the temperature values at other positions. Fig. 6 shows the fuzzy coordination control system that employs two synergic PID controllers to simultaneously adjust the bypass and the exposing degree of the radiator. Unlike the separate PID control that manipulates only one of two variables $u \in \{\varphi_b, \mu_r\}$, the fuzzy coordinate control (FCC) includes a fuzzy decision unit (FDU) to derive a coordination factor λ that takes the actuator characteristics into account.

Synergic PID Controllers

The control law for the synergic PID controllers is given by (17), where the coordination factor λ is determined by the FDU

$$\begin{bmatrix} \varphi_{b,k} \\ \mu_{r,k} \end{bmatrix} = \begin{bmatrix} \varphi_{b,k-1} \\ \mu_{r,k-1} \end{bmatrix} + \begin{bmatrix} \lambda_k & 0 \\ 0 & 1-\lambda_k \end{bmatrix} \begin{bmatrix} \Delta\varphi_{b,k} \\ \Delta\mu_{r,k} \end{bmatrix} \tag{17}$$

where the subscripts "k" and "$k-1$" represent values evaluated at the current and previous sampling instants, respectively, (K_p, T_i, T_d) are the proportional gain and the integral and differential time constants of the PID controllers, respectively, and T_s is the sampling period. In (5), the incremental manipulating values ($\Delta\varphi_{b,k}$ and $\Delta\mu_{r,k}$ for the bypass and louver) are given in terms of PID gains

$$\begin{bmatrix} \Delta\varphi_{b,k} \\ \Delta\mu_{r,k} \end{bmatrix} = \begin{bmatrix} K_{\rm pb}\left\{\Delta e_k + \frac{T_s}{T_{\rm ib}} e_k + \frac{T_{\rm db}}{T_s}\left(\Delta e_k - \Delta e_{k-1}\right)\right\} \\ K_{\rm pr}\left\{\Delta e_k + \frac{T_s}{T_{\rm ir}} e_k + \frac{T_{\rm dr}}{T_s}\left(\Delta e_k - \Delta e_{k-1}\right)\right\} \end{bmatrix} \tag{18}$$

where $\Delta e_k = e_k - e_{k-1}$.

FDU

The FDU consists of a fuzzifier transforming e_k and Δe_k into fuzzy values, an inference engine reasoning upon linguistic rules in a database, and a defuzzifier that transforms the FDU output into a real crisp number λ_k to provide single-valued control signals for the plant. The fuzzy decision rule at the kth sampling instant has the following form:

$$\text{IF } e_k \text{ is } E_i \text{ and } \Delta e_k \text{ is } CE_j, \text{ THEN } \lambda_k \text{ is } DE_{\ell(i,j)} \tag{19}$$

where E_i, CE_j, and $DE_{\ell(i,j)}$ are the fuzzy sets reflecting the linguistic values of e_k, Δe_k, and λ_k, respectively, and the subscript variables i, j, and $\ell(i,j)$ denote the analytical rank associated with the linguistic values in a nine-element set $\{\text{NS}, \text{NH}, \text{NM}, \text{NL}, \text{ZE}, \text{PL}, \text{PM}, \text{PH}, \text{PS}\}$ defined in Fig. 7. Gaussian membership functions, which overlap with each other to provide a smooth output transition between regions, are used to define the linguistic values in both the fuzzifier and defuzzifier.

The coordinate factor output from the FDU is given by the following defuzzification algorithm which takes the form

$$\lambda_k = \sum_{i=1}^{9}\sum_{j=1}^{9} \lambda_{\ell(i,j)}\eta_{\ell(i,j)} \Big/ \sum_{i=1}^{9}\sum_{j=1}^{9} \eta_{\ell(i,j)}. \tag{20}$$

In (20), $\lambda_{\ell(i,j)}$ and $\eta_{\ell(i,j)}$ are the discrete element and membership degree of the output fuzzy set $DE_{\ell(i,j)}$ representatively.

Fuzzy Rule Design Considerations

The fuzzy control law is designed to overcome problems associated with separate louver or T-valve PID controls which exhibit the following disadvantages.

1) Frequent adjustment of MEMS louvers (on the outer surface of the space radiator in the space environment) could significantly reduce the reliability of the thermal control system.

TABLE IV
FUZZY DECISION RULES

E_i/CE_j	NS	NH	NM	NL	ZE	PL	PM	PH	PS
NS	ZE	ZE	ZE	PL	PL	PL	ZE	ZE	ZE
NH	ZE	PL	PL	PL	PL	PL	PL	PL	ZE
NM	ZE	PL	PM	PM	PH	PM	PM	PL	ZE
NL	PL	PL	PM	PH	PS	PH	PM	PL	PL
ZE	PL	PL	PH	PS	PS	PS	PH	PL	PL
PL	PL	PL	PM	PH	PS	PH	PM	PL	PL
PM	ZE	PL	PM	PM	PH	PM	PM	PL	ZE
PH	ZE	PL	PL	PL	PL	PL	PL	PL	ZE
PS	ZE	ZE	ZE	PL	PL	PL	ZE	ZE	ZE

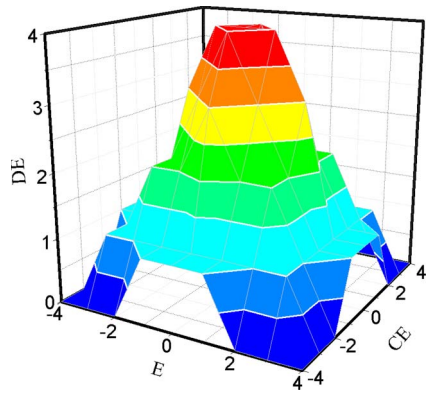

Fig. 8. Surface map of the fuzzy decision rules.

2) Dynamical response is much slower than the PID control with the bypass channel of the T-valve.
3) The fast bypass-based PID control, however, could introduce some undesired hydraulic disturbances in the MHEs and is only suitable for applications where disturbances are small.

Based on the aforementioned considerations, the fuzzy rules are designed such that the T-valve controller is given a more important role when the control error and its variation rate are relatively small. On the other hand, the louver controller dominates when they are large. Thus, a large coordinating factor λ to the T-valve controller is required for small control error and small error variation rate and vice versa.

For the two-input system (e_k and Δe_k, each with nine linguistic values given in Fig. 7), a fully populated rule base will have $9 \times 9 = 81$ input rule combinations. The rank-based fuzzy decision rules are constructed using the rule generating policy in

$$l(i,j) = \text{nInt}\left(\alpha \exp\left(-(i^2+j^2)/\beta\right)\right) \tag{21}$$

where the function nInt(x) rounds off x to its nearest integer number and the parameter values of α and β are set to four and nine. The rules are listed in Table IV and graphically shown in Fig. 8.

IV. RESULTS AND DISCUSSION

The FCC is numerically evaluated in terms of the dynamic response to a 10% step reduction in the input heat load Q_1 to MHEx-1. The results, which examine the closed-loop control effects, are compared against two single-input PID controls which serve as a basis for comparison.

TABLE V
PARAMETERS OF THE SIMULATED CONTROLLERS

Fuzzy coordinate control (III)			Separate PID control		
Parameters	T-valve	Radiator	Parameters	PID (I)	PID (II)
$K_{pb(r)}$	0.6	-0.4	K_p	0.6	-0.4
$T_{ib(r)}$	20	20	T_i	20	20
$T_{db(r)}$	0	0	T_d	0	0
Sampling period, T_s=1.0 second.					

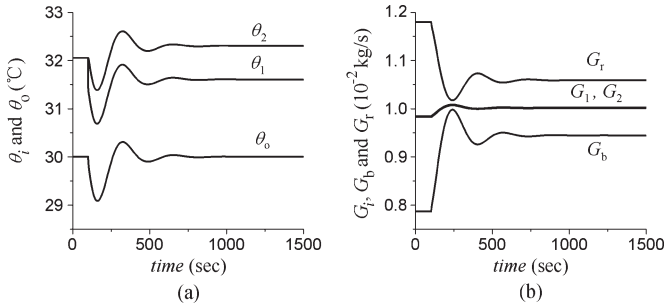

Fig. 9. Simulated responses of FCC. (a) Hot circuit temperature. (b) Mass flow rate.

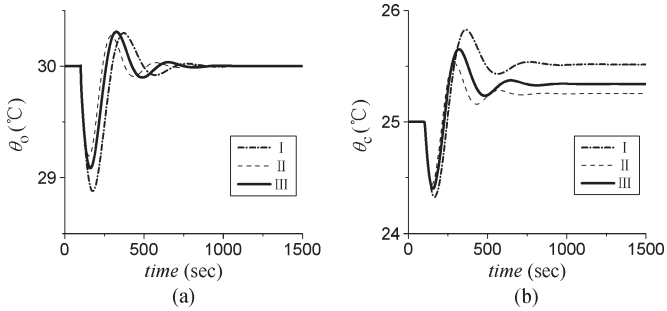

Fig. 10. Working fluid temperatures. (a) Hot circuit outlet. (b) Cold circuit outlet.

1) **PID (I)**: T-valve bypass as manipulating variable.
2) **PID (II)**: Radiator exposing degree as manipulator variable. Note that no mass flow is manipulated in PID (II).
3) **FCC (III)**: Synergic control of T-valve and exposing radiator degree.

The values of the control parameters used in the simulation are summarized in Table V.

The temperature responses in the hot circuit and the mass flow rate responses in the cooling network under FCC are shown in Fig. 9(a) and (b), respectively. Comparisons against the two classical PID single-input controllers are shown in Figs. 10–13. The closed-loop overshoots and settling times (1% criterion) of the simulated transients are summarized in Table VI and are denoted as γ and τ, respectively.

Some major observations are summarized as follows.

1) As shown in Fig. 9(a), FCC (III) achieves the objective of maintaining θ_o as expected. The new steady-state temperatures of MHEx-1 and MHEx-2 are within 0.5 °C from their initial operating values. This small variation is due to the fact that MHEx-1 and MHEx-2 in the hot

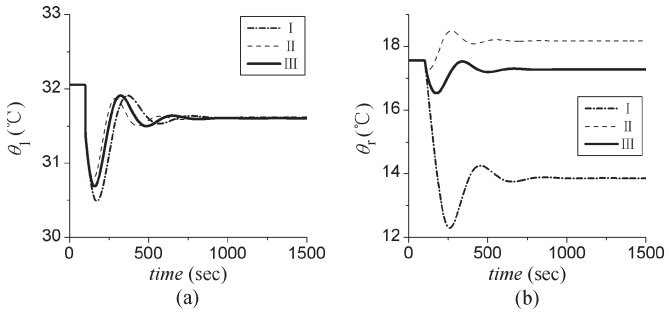

Fig. 11. Heat exchanger temperatures. (a) MHEx-1. (b) Radiator.

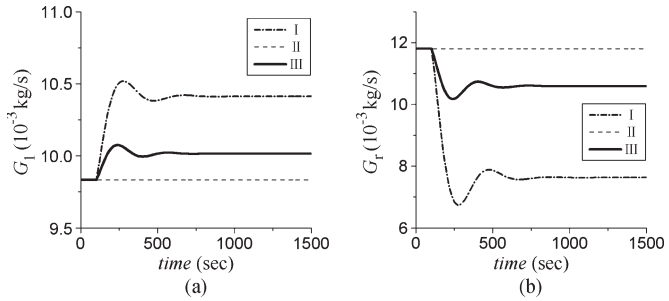

Fig. 12. Mass flow rate responses. (a) MHEx-1. (b) Radiator.

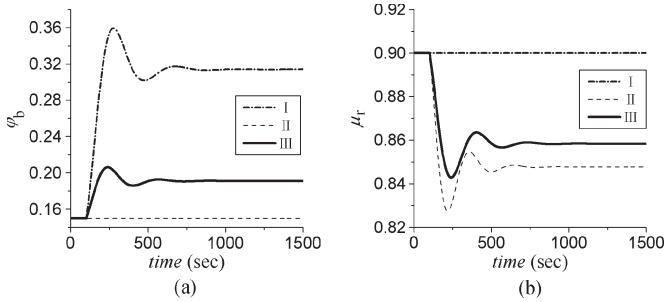

Fig. 13. Changes in manipulating variables. (a) Bypass valve value. (b) Exposing degree of radiator.

TABLE VI
CLOSED-LOOP OVERSHOOTS AND SETTLING TIMES

	PID (I)		PID (II)		FCC (III)	
	γ(%)	τ (sec)	γ(%)	τ (sec)	γ(%)	τ (sec)
θ_o	0.98	172	0.91	113	0.99	134
θ_c	1.22	298	1.02	196	1.22	259
θ_l	-3.55	163	-2.55	103	-2.92	124
θ_r	-11.09	447	1.52	212	-4.11	280
G_l	1.02	197	-	-	0.58	53
G_r	-11.65	575	-	-	-3.92	340
φ_b	14.59	590	-	-	7.70	458
μ_r	-	-	-2.35	255	-1.82	191

circuit experience less than 2% changes in flow rates, as shown in Fig. 9(b). Flow rate changes primarily occur in MHEx-c (10%) and the bypass (20%) in the cold circuit as designed.

2) As shown in Figs. 10(a) and 11(a), all three schemes achieve the control objective of maintaining θ_o. PID (II) and FCC (III), however, offer a better temperature dynamic performance than PID (I) [as shown in Figs. 10(b) and 11(b)] in rejecting disturbances in Q_1. The overshoot of θ_r in FCC (III) is reduced to 37.1% of that in PID (I) according to the values in Table VI. This will benefit the safe operation of the MEMS radiator.
3) FCC (III) demonstrates an excellent flow rate management ability as compared to PID (I) in Fig. 12; the variation of flow rate G_r through MHEx-c has been reduced by 70%, and the settling time has been shortened to 59.1% when the radiator, in addition to T-valve, is manipulated through FCC.
4) More importantly, FCC (III) keeps the T-valve and radiator from being overmanipulated. As shown in Fig. 13, changes in φ_b and μ_r are within 27% and 5% of their initial values, respectively. As a comparison, FCC (III) requires only 25% of φ_b for PID (I), where only the T-valve is manipulated, while the value of μ_r for FCC reduces to 80% of that for PID (II) with only radiator control. It is worth noting that, unlike FCC (III), either PID (I) or PID (II) cannot simultaneously control the actions of the T-valve and radiator.

V. CONCLUSION

The thermohydraulic model, dynamic analysis, and fuzzy coordination (FCC) control of a single-phase MHE cooling network for space electronics have been presented. Specifically, the network consists of a flow-based control mechanism through a T-valve bypass and a radiation-based MEMS louver array for cooling space electronics. Models for calculating the fluid distribution and temperature transient in an MHE space cooling network have been derived. These models provide a basis for developing an FCC strategy for manipulating the T-valve bypass value and the exposing degree of the radiator simultaneously.

Numerical investigations on both open- and closed-loop performances suggest that the T-valve can provide a relatively rapid rejection to small disturbances and that the radiator louvers are more effective for gradually settling larger disturbances. The FCC system results in excellent temperature control effects, less mass flow rate disturbances, and a smoother trajectory in the manipulating variables. The results have also demonstrated that the FCC is more reliable and robust than two separate PID control approaches by avoiding frequent adjustments of the T-valve and radiator and by intelligently changing the coordinating factor based on the varying control situations.

While the analysis and fuzzy coordination control are presented in the context of space cooling networks, it is expected that the methods presented here will have potential applications in other thermal control systems where MHEs and forced liquid cooling technologies are employed.

APPENDIX

The fluid flow in the microchannels is typically in the range of laminar flow (Reynolds number N_{Re} less than 2300). The

friction factor and heat transfer coefficient of the MHE are given in [1]

$$f = (4.7 + 19.64G)/N_{\mathrm{Re}} = (\Delta P/L)D_h(0.5\rho_f v^2)^{-1} \quad \text{(A.1)}$$

$$h = k_f(-1.047 + 9.326G)/D_h \quad \text{(A.2)}$$

where k_f, ρ_f, and v are the thermal conductivity, the density, and the flowing speed of the working fluid, respectively, and the geometric parameter and hydraulic diameter are given by

$$G = \frac{r_w^2 + 1}{(r_w + 1)^2} \quad \text{(A.3a)}$$

$$\frac{D_h}{D} = \frac{2r_w}{1 + r_w} \quad \text{(A.3b)}$$

where $r_w = w_c/D$.

The equation for calculating the flow resistance though an MHE can be deduced from (A.1)

$$R = 0.5(L/D_h)(4.7 + 19.64G)(N_{\mathrm{Re}})^{-1}(\rho_f A^2)^{-1} \quad \text{(A.4)}$$

where A is the cross-sectional area of the microchannels in MHEs.

REFERENCES

[1] L. Meysenc, L. Saludjian, A. Bricard, S. Rael, and C. S Chaeffer, "A high heat flux IGBT micro exchanger setup," *IEEE Trans. Compon., Packag., Manuf. Technol. A*, vol. 20, no. 3, pp. 334–341, Sep. 1997.

[2] D. Lorenzen, J. Bonhaus, W. R. Fahrner, E. Kaulfersch, E. Worner, P. Koidl, K. Unger, D. Muller, S. Rolke, H. Schmidt, and M. Grellmann, "Micro thermal management of high-power diode laser bars," *IEEE Trans. Ind. Electron.*, vol. 48, no. 2, pp. 286–297, Apr. 2001.

[3] J. Schutze, H. Ilgen, and W. R. Fahrner, "An integrated micro cooling system for electronic circuits," *IEEE Trans. Ind. Electron.*, vol. 48, no. 2, pp. 281–285, Apr. 2001.

[4] A. D. Paris, G. C. Birur, and A. A. Green, "Development of MEMS microchannel heat sinks for micro/nano spacecraft thermal control," presented at the ASME Int. Mechanical Engineering Congr. and Expo., New Orleans, LA, 2002, Paper IMECE-2002-34293.

[5] G. C. Birur and P. Bhandari, "Mars pathfinder active heat rejection system: Successful flight demonstration of a mechanically pumped cooling loop," presented at the 28th Int. Conf. Environmental Systems, Danvers, MA, 1998, Paper SAE-981684.

[6] R. Osiander, S. L. Firebaugh, L. Champion, D. Farrar, and M. A. G. Darrin, "Micro electromechanical devices for satellite thermal control," *IEEE Sensors J.*, vol. 4, no. 4, pp. 525–531, Aug. 2004.

[7] D. Farrar, W. Schneider, R. Osiander, J. L. Champion, A. G. Darrin, and D. Douglas, "Controlling variable emittance (MEMS) coatings for space applications," in *Proc. 8th Intersoc. Conf. Therm. Thermomech. Phenom. Electron. Syst.*, 2002, pp. 1020–1024.

[8] G. Birur, P. Shakkottai, and T. W. Sur, "MEMS based pumped liquid cooling system for micro/nano spacecraft thermal control," in *Proc. Int. Conf. Nano/Micro Technol. Space Biomed. Appl.*, Galveston, TX, 2001, pp. 11–22.

[9] D. Liu and S. V. Garimellam, "Investigation of liquid flow in microchannels," *J. Thermophys. Heat Transf.*, vol. 18, no. 1, pp. 65–72, 2004.

[10] W. Lou, X. Yu, and B. Qi, "The simulation for pressure loss of microchannel heat sinks inlet," in *Proc. 2nd IEEE Int. Conf. Nano/Micro Eng. Molec. Syst.*, Jan. 2007, pp. 1–6.

[11] P.-S. Lee, S. V. Garimella, and D. Liu, "Investigation of heat transfer in rectangular microchannels," *Int. J. Heat Mass Transf.*, vol. 48, no. 9, pp. 1688–1704, Apr. 2005.

[12] D. P. Kulkarni and D. K. Das, "Analytical and numerical studies on microscale heat sinks for electronic applications," *Appl. Therm. Eng.*, vol. 25, no. 14/15, pp. 2432–2449, Oct. 2005.

[13] M. Iyengar and S. Garimella, "Design and optimization of microchannel cooling systems," in *Proc. 10th Intersoc. Conf. Therm. Thermomech. Phenom. Electron. Syst.*, 2006, pp. 54–62.

[14] H. S. Park, J. I. Jo, J. Y. Chang, and S. S. Kim, "Methodology of optimization for microchannel heat exchanger," in *Proc. 22nd Annu. IEEE Semicond. Therm. Meas. Manage. Symp.*, 2006, pp. 65–68.

[15] J. R. Schmidt and D. R. Clark, "Analog simulation technique for modeling parallel-flow heat exchangers," *IEEE Trans. Power App. Syst.*, vol. PAS-87, no. 5, pp. 1300–1305, May 1968.

[16] M. Baldea and P. Daoutidis, "Model reduction and control of reactor–heat exchanger networks," *J. Process Control*, vol. 16, no. 3, pp. 265–274, Mar. 2006.

[17] A. H. González, D. Odloak, and J. L. Marchetti, "Predictive control applied to heat-exchanger networks," *Chem. Eng. Process.*, vol. 45, no. 8, pp. 661–671, Aug. 2006.

[18] K.-M. Lee and Y. Qian, "A vision-guided fuzzy logic control system for dynamic pursuit of moving target," *Microprocess. Microsyst.*, vol. 21, no. 9, pp. 571–580, Apr. 1998.

[19] G. C. D. Sousa, B. K. Bose, and J. G. Cleland, "Fuzzy logic based on-line efficiency optimization control of an indirect vector-controlled induction motor drive," *IEEE Trans. Ind. Electron.*, vol. 42, no. 2, pp. 192–198, Apr. 1995.

[20] T. Orlowska-Kowalska, M. Dybkowski, and K. Szabat, "Adaptive sliding-mode neuro-fuzzy control of the two-mass induction motor drive without mechanical sensors," *IEEE Trans. Ind. Electron.*, vol. 57, no. 2, pp. 553–564, Feb. 2010.

[21] M. A. Fnaiech, F. Betin, G.-A. Capolino, and F. Fnaiech, "Fuzzy logic and sliding-mode controls applied to six-phase induction machine with open phases," *IEEE Trans. Ind. Electron.*, vol. 57, no. 1, pp. 354–364, Jan. 2010.

[22] J.-W. Kim and S. W. Kim, "Design of incremental fuzzy PI controllers for a gas-turbine plant," *IEEE/ASME Trans. Mechatronics*, vol. 8, no. 3, pp. 410–414, Sep. 2003.

[23] H. Rouhani, M. Jalili, B. N. Araabi, W. Eppler, and C. Lucas, "Brain emotional learning based intelligent controller applied to neurofuzzy model of micro-heat exchanger," *Exp. Syst. Appl.*, vol. 32, no. 3, pp. 911–918, Apr. 2007.

[24] C.-F. Juang and J.-S. Chen, "Water bath temperature control by a recurrent fuzzy controller and its FPGA implementation," *IEEE Trans. Ind. Electron.*, vol. 53, no. 3, pp. 941–949, Jun. 2006.

[25] Y.-Z. Li, K.-M. Lee, and J. Wang, "Analysis and control of equivalent physical simulator for nanosatellite space radiator," *IEEE/ASME Trans. Mechatronics*, vol. 15, no. 1, pp. 79–87, Feb. 2010.

[26] D. G. Gilmore, *Spacecraft Thermal Control Handbook*, 2nd ed. Los Angeles, CA: Aerospace Press, 2002, ch. 19.

Yun-Ze Li (M'09) received the B.S. degree in thermal and electrical engineering from North China University of Water Conservancy and Electric Power, Zhengzhou, China, in 1996, the M.S. degree in thermal power engineering from Xi'an Jiaotong University, Xi'an, China, in 2000, and the Ph.D. degree in engineering thermal physics from Tsinghua University, Beijing, China, in 2002.

From 1996 to 1997, he was an Assistant Engineer with Xingtai Power Corporation, Hebei, China. From 2003 to 2004, he was a Postdoctoral Researcher at Beijing University of Aeronautics and Astronautics, Beijing. He is currently a Professor in the School of Aeronautical Science and Engineering, Beihang University, Beijing, China. He was a Visiting Scholar at Georgia Institute of Technology, Atlanta, in 2007, and at National Cheng Kung University, Tainan City, Taiwan, in 2008. His current major research interests include thermal control and energy management of aerospace systems.

Kok-Meng Lee (M'89–SM'02–F'05) received the B.S. degree from the State University of New York, Buffalo, in 1980, and the S.M. and Ph.D. degrees from Massachusetts Institute of Technology, Cambridge, in 1982 and 1985, respectively.

He is currently a Professor in The George W. Woodruff School of Mechanical Engineering, Georgia Institute of Technology, Atlanta. His research interests include system dynamics/control, robotics, automation, and mechatronics. He is the holder of eight patents in machine vision, a three-degree-of-freedom spherical motor/encoder, and a live-bird handling system.

Prof. Lee is a Fellow of the American Society of Mechanical Engineers. He was the recipient of the National Science Foundation Presidential Young Investigator Award, the Sigma Xi Junior Faculty Research Award, the International Hall of Fame New Technology Award, and the Kayamori Best Paper Award.